STAR★METHODS

KEY RESOURCES TABLE

REAGENT or RESOURCE	SOURCE	IDENTIFIER
Antibodies		
pMEK (rabbit monoclonal, anti-human)	Cell Signaling	9154S
pERK (rabbit monoclonal, anti-human)	Cell Signaling	4370L
pAkt (rabbit monoclonal, anti-human)	Cell Signaling	4060L
Actin (rabbit monoclonal, anti-human)	Sigma	101M4755
GFP (rabbit monoclonal)	Cell Signaling	2956S
GFP (rabbit monoclonal) for EM-immuno-labeling	Hancock Lab	N/A
RFP (rabbit monoclonal) for EM-immuno-labeling	Hancock lab	N/A
Chemicals, Peptides, and Recombinant Proteins		
Brain PtdSer	Avanti Polar Lipids	840032C
Di18:1 PtdSer	Avanti Polar Lipids	840035C
Di18:2 PtdSer	Avanti Polar Lipids	840040C
16:0/18:1 PtdSer	Avanti Polar Lipids	840034C
18:0/18:1 PtdSer	Avanti Polar Lipids	840039C
TopFluor PtdSer	Avanti Polar Lipids	810283C
R-Fendiline	Synthesized by the Translational Chemistry Core Facility at M. D. Anderson Cancer Center	https://mdanderson.influuent.utsystem.edu/en/equipments/translational-chemistry-core-facility-tccf
cGMP	Enzo	BML-CN205-0050
DMEM	GIBCO	10569-010
F-12K medium	Corning	10-025-CV
FBS	GIBCO	16000-044
Dialyzed FBS	GIBCO	26400-036
BCS	Hyclone	SH30072.03
Trypsin-EDTA (0.5%)	GIBCO	15400-054
Trypsin-EDTA (0.25%)	GIBCO	25200-072
Aproptinin	Sigma	A6279-5ML
Na_3VO_4	Sigma	S6508-50G
Leupeptin	Sigma	L2884-25MG
DTT	Sigma	D9779-5G
Tris base	J. T. Baker	4109-06
SDS	Fisher	BP166-500
bromophenol blue dye	Sigma	B8026-25G
Acrylamide (30%)	Bio-Rad	161-0158
Ammonium persulfate	Sigma	A9164-100G
Tetramethylethylenediamine	Sigma	T-7024
polyvinylidene difluoride (PVDF) membrane	Fisher	NEF-1002001PK
NaCl	Sigma	S7653-5KG
Coomassie BrilliNR Blue	Sigma	BP101-50
Methanol	Sigma	179337-4L
Glacial acetic acid	Fisher	BP2401-212
Skim milk	MP Biomedicals	902887
NP40	Sigma	I8896-100ML

(*Continued on next page*)

Continued

REAGENT or RESOURCE	SOURCE	IDENTIFIER
Tween 20	Sigma	P1379-1L
SuperSignal West Pico stable peroxide solution	Thermo Scientific	1856135
SuperSignal West Dura stable peroxide solution	Thermo Scientific	1859025
Pioloform	TED PELLA	19244
Choroform	Electron Microscopy Sciences (EMS)	12550
Poly-L-lysine	Sigma	P8920-100ML
EM copper grids	EMS	G200-CU
Trisodium citrate	Sigma	C3674-100G
Tannic acid	EMS	21710
Potassium carbonate	Sigma	P5833-500G
Potassium acetate	Sigma	P1190-1KG
Glycerol	Sigma	G55-1L
Paraformalgehyde	EMS	1570
Glutaraldehyde	EMS	16220
Fish gelatin	Sigma	G7765-250ML
BSA	Sigma	A6003-100G
Gold chloride	Sigma	254169-5G
Lipofectamine	Invitrogen	50470
Lipofectamine 2000	Invitrogen	11668-500
Opti-MEM	GIBCO	31985-070
Polyvinyl alcohol 4-88 (Mowiol)	Fluka	81381
Critical Commercial Assays		
Reversed phase protein array	M. D. Anderson Cancer Center RPPA core	https://www.mdanderson.org/research/research-resources/core-facilities/functional-proteomics-rppa-core.html
Lipidomics	Lipotype	https://www.lipotype.com
Experimental Models: Cell Lines		
Baby hamster kidney (BHK) cells	Gift of Dr. Robert G. Parton (University of Queensland, Australia) Zhou et al., 2014	N/A
Mardin-Darby canine kidney (MDCK) cells	Gift of Dr. Robert G. Parton (University of Queensland, Australia) Cho et al., 2015	N/A
Chinese ovarian PSA-3 cells	Gift of Dr. Tomohiko Taguchi (University of Tokyo, Japan) Lee et al., 2012	N/A
Recombinant DNA		
GFP-K-RasG12V	Zhou et al., 2015	N/A
GFP-K-RasG12V-K175Q	This paper	N/A
GFP-K-RasG12V-K176Q	This paper	N/A
GFP-K-RasG12V-K177Q	This paper	N/A
GFP-K-RasG12V-K178Q	This paper	N/A
GFP-K-RasG12V-K179Q	This paper	N/A
GFP-K-RasG12V-K180Q	This paper	N/A
GFP-K-RasG12V-6R	This paper	N/A
GFP-K-RasG12V-CCIL	This paper	N/A
GFP-K-RasG12V-6R,CCIL	This paper	N/A

(*Continued on next page*)

Continued

REAGENT or RESOURCE	SOURCE	IDENTIFIER
GFP-tK	Zhou et al., 2015	N/A
GFP-tK-K175Q	This paper	N/A
GFP-tK-K176Q	This paper	N/A
GFP-tK-K177Q	This paper	N/A
GFP-tK-K178Q	This paper	N/A
GFP-tK-K179Q	This paper	N/A
GFP-tK-K180Q	This paper	N/A
RFP-K-RasG12V	Zhou et al., 2015	N/A
RFP-K-RasG12V-K175Q	This paper	N/A
RFP-K-RasG12V-K176Q	This paper	N/A
RFP-K-RasG12V-K177Q	This paper	N/A
RFP-K-RasG12V-K178Q	This paper	N/A
RFP-K-RasG12V-K179Q	This paper	N/A
RFP-K-RasG12V-K180Q	This paper	N/A
RFP-tK	Zhou et al., 2015	N/A
RFP-tK-K175Q	This paper	N/A
RFP-tK-K176Q	This paper	N/A
RFP-tK-K177Q	This paper	N/A
RFP-tK-K178Q	This paper	N/A
RFP-tK-K179Q	This paper	N/A
RFP-tK-K180Q	This paper	N/A
RFP-tK-CCIL	This paper	N/A
Software and Algorithms		
NAMD2.9 and 2.10	Dr. Klaus Schulten (free software and publically available)	http://www.ks.uiuc.edu/Research/namd
COLVARS	Dr. Klaus Schulten (free software and publically available)	http://www.ks.uiuc.edu/Research/vmd/current/ug/node233.html
VMD-1.9.1	Dr. Klaus Schulten (free software and publically available)	http://www.ks.uiuc.edu/Research/vmd/
OriginPro2016	OriginLab	http://www.originlab.com/
GIMP2.8	GNU Image Manipulation program (free software)	https://www.gimp.org/
K_Function_UNIVARIATE	Hancock lab	N/A
K_Function_BIVARIATE	Hancock lab	N/A
BIV_LOOKUP_TABLE	Hancock lab	N/A
K-RAS_PM_Image J_MACRO	Hancock lab	N/A

CONTACT FOR REAGENT AND RESOURCE SHARING

Further information and requests for reagents may be directed to, and will be fulfilled by corresponding author John F. Hancock (john.f.hancock@uth.tmc.edu).

EXPERIMENTAL MODEL AND SUBJECT DETAILS

Culture Conditions for In Vitro Systems

BHK cells were maintained in DMEM containing 10% BCS. MDCK cells were maintained in DMEM containing 10% FBS. PSA3 cells were maintained in F-12K medium containing 10% FBS and supplemented with 10 μM ethanolamine (Etn). For PtdSer depletion, PSA3 cells were grown in F-12K medium containing 10% dialyzed FBS (DFBS) for 72 hr. In experimental control cultures wild-type levels of PtdSer were maintained by growing PSA3 cells in F-12K medium containing 10% DFBS supplemented with 10 μM Etn for 72 hr (Cho et al., 2015; Lee et al., 2012; Zhou et al., 2014).

To generate stable cell lines 4x10^5 MDCK cells were seeded in a 3.5 cm dish on day 1. When the cell confluency reached ~95% on day 2, 4 μg plasmid DNA with pEF6 promoter was mixed with 10 μL Lipofectamine 2000 for 20 min and then added to cells. After overnight incubation, plasmid DNA / lipofectamine 2000 mixture was aspirated off and switched to complete medium (DMEM with 10% FBS). Antibiotic blasticidin at 10 μg/ml was used for selection. MDCK cells were then passaged 3-4 times before serial dilution, where cells were diluted to ~5–7 cells/ml and 100 μL of diluted cell suspension was added to each well in a 96-well plate. Typically three 96-well plates were used for each cell line. At least 8 colonies were picked after ~2 weeks of growing in 96-well plates with the aid of a wide-field fluorescence microscope. Each colony was seeded in a 3.5 cm dish with glass bottom for confocal imaging. Cell lines expressing uniform level of GFP-tagged proteins were picked. Typically, steps between serial dilution and confocal imaging were repeated 2-3 times to obtain the best monoclonal colony with the optimal and uniform expression of GFP-tagged proteins.

For transient expression BHK cells were seeded at a density of ~1.4x10^6 cells/ml in 3.5 cm dishes on day 1. On day 2, 0.8 μg of plasmid DNA construct(s) of interest (incorporated in a vector containing CMV promoter) was mixed with 7 μL of lipofectamine (2 mg/ml) in 1 ml of Opti-MEM. After incubation of 20 min in a 5 ml polystyrene tube, the mix was carefully pipetted into a 3.5 cm dish containing cells. Lipofectamine, cDNA and Opti-MEM mix was aspirated off after 5 hr incubation, which was then followed by overnight incubation with DMEM medium containing 10% BCS.

METHOD DETAILS

EM-Spatial Mapping to Quantify the Extent of Nanoclustering and Co-localization of Proteins and Lipids on the Plasma Membrane

(a) Univariate K-Function Analysis to Examine the Spatial Distribution of a Single Species on the Plasma Membrane

This methodology quantifies the extent of lateral spatial segregation of proteins or lipids in the inner leaflet of cell plasma membrane (Prior et al., 2003a, 2003b). BHK cells were seeded on glass coverslips with a density of approximately 1.4x10^5 cells/ml of medium on day 1, transiently transfected with a GFP-tagged protein/peptide of interest on day 2. Approximately 18 hr after transfection (on day 3) and any experimental treatment, cells were washed twice with PBS at room temperature. Two copper EM grids, which are pre-coated with pioloform and poly-L-lysine, were placed on top of the cells with the coated surface in contact with the cells. Apical plasma membrane (PM) was attached to the EM grids by pressing down on the grids with a large rubber bung. This was followed by pipetting ~100 μL potassium acetate (KOAc) buffer (115 mM KOAc, 5 mM $MgCl_2$ and 25 mM HEPES at pH7.4) onto the glass coverslip. Surface pressure of the buffer solution lifts the grids off the glass coverslip, bringing attached apical PM. The EM copper grids were then sequentially positioned on bubbles of 50 μL fixative agents (4% paraformaldehyde and 0.1% glutaraldehyde dissolved in KOAc buffer, 10 min), 100 μL PBS (5 min), 3 sequential 100 μL quenching solution (20 mM glycine, 5 min each time), 100 μL blocking solution (0.2% fish skin gelatin and 0.2% BSA in PBS, 20 min). Fixed PM sheets attached to the EM grids were then immunogold-labeled by incubating with 10.5 μL of gold antibody solution (4.5 nm gold conjugated to anti-GFP antibody) for 30 min before being placed on 5 sequential 100 μL bubbles of blocking solution (5 min each time) and then 5 sequential 100 μL bubbles of deionized water. EM grids were then placed on 100 μL bubbles of negative staining solution (0.3% uranyl acetate dissolved in 2% methyl cellulose) for 9 min. An EM grid loop was used to scoop the grid up from the staining solution, with excess uranyl acetate being blotted off using filter paper. The EM grids were then left on the loops overnight to dry before imaging.

Intact and featureless PM sheets were imaged using a JEOL JEM-1400 transmission EM at 100,000X magnification. ImageJ was used to assign x and y coordinates to gold particles in a 1-μm^2 area of interest on a PM sheet. We use Ripley's K-function to quantify the gold particle distribution and the extent of nanoclustering (Equations A and B):

$$K(r) = An^{-2}\sum_{i\neq j} w_{ij} 1(\|x_i - x_j\| \leq r) \quad \text{(Equation A)}$$

$$L(r) - r = \sqrt{\frac{K(r)}{\pi}} - r \quad \text{(Equation B)}$$

where $K(r)$ is the univariate K-function for a distribution of n points in an area A; r = length scale with the range of $1 < r < 240$ nm at 1-nm increments; $\|\cdot\|$ is Euclidean distance; $1(\cdot)$ is the indicator function with a value of 1 if $\|x_i - x_j\| \leq r$ and a value of 0 otherwise; and w_{ij}^{-1} is the proportion of the circumference of the circle with center x_i and radius $\|x_i - x_j\|$ contained within the selected PM area A (we include as an unbiased edge correction for points at the edge of the study area). $L(r) - r$ is a linear transformation of $K(r)$. Here $L(r) - r$ is normalized on the 99% confidence interval (99% C.I.) estimated from Monte Carlo simulations. Under the null hypothesis of complete spatial randomness $L(r) - r$ has an expected value of 0 for all values of r. Positive deviations of the function outside of the confidence interval therefore indicate significant clustering. The maximum value of the $L(r) - r$ function is an excellent summary statistic that correlates with the extent of clustering (Plowman et al., 2005). For each condition in this study, at least 15 PM sheets were imaged, analyzed and the data pooled. Data S1 includes a custom algorithm to calculate the univariate K-function.

Bootstrap tests were used to evaluate differences between replicated point patterns. For this purpose we use the statistic *D*:

$$D = \sum_{i=1}^{g} \int_{10}^{110} w(r) n_i [K_i(r) - K(r)]^2 dr \qquad \text{(Equation C)}$$

where $w(r) = r^{-2}$, $K_i(r)$ = weighted mean K-function of the i^{th} group of size n_i, and $K(r)$ = combined weighted mean K-function of all the groups being compared (g). The observed value of D was ranked against 1000 Monte Carlo simulated values of D calculated using a set of residual K-functions derived from each $K_i(r)$ (Diggle et al., 2000; Plowman et al., 2005)

(b) Bivariate K-Function Analysis to Quantify the Extent of Co-clustering / Co-localization between Two Different Species on the Plasma Membrane

The bivariate K-function analyzes co-clustering / co-localization of two populations of proteins / peptides on the PM inner leaflet. BHK cells were seeded on glass coverslips with a density of ~1.4x10^5 cells/ml of medium on day 1, transiently co-transfected with GFP- and RFP-tagged proteins/peptides of interest on day 2. Approximately 18 hr after transfection (on day 3) and any experimental treatments, PM sheets were prepared and fixed exactly as described in the previous section. Fixed PM sheets attached to the EM grids were then immuogold-labeled by incubating with 10.5 μL of gold solution (6 nm gold conjugated to anti-GFP antibody) for 30 min, followed by incubation on a 100 μL bubble of blocking solution (5 min) and then 10.5 μL of gold solution containing 2 nm gold conjugated to anti-RFP antibody (30 min). EM grids were then positioned on 5 sequential 100 μL bubbles of blocking solution (5 min each time) and then 5 sequential 100 μL bubbles of deionized water. EM grids were then placed on 100 μL bubbles of negative staining solution (0.3% uranyl acetate dissolved in 2% methyl cellulose) for 9 min. An EM grid loop was used to scoop the grid up from the staining solution, with excess uranyl acetate being blotted off using filter paper. The EM grids were then left on the loops overnight to dry before imaging.

Intact PM sheets were imaged using a JEOL JEM-1400 transmission EM and ImageJ used to assign x and y coordinates to each separate population of gold particles in a 1-μm^2 area of interest on a PM sheet. Gold particle co-localization was analyzed using bivariate K-functions. (Equations D–G):

$$K_{biv}(r) = (n_b + n_s)^{-1} [n_b K_{sb}(r) + n_s K_{bs}(r)] \qquad \text{(Equation D)}$$

$$K_{bs}(r) = \frac{A}{n_b n_s} \sum_{i=1}^{n_b} \sum_{j=1}^{n_s} w_{ij} 1(\| x_i - x_j \| \leq r) \qquad \text{(Equation E)}$$

$$K_{sb}(r) = \frac{A}{n_b n_s} \sum_{i=1}^{n_s} \sum_{j=1}^{n_b} w_{ij} 1(\| x_i - x_j \| \leq r) \qquad \text{(Equation F)}$$

$$L_{biv}(r) - r = \sqrt{\frac{K_{biv}(r)}{\pi}} - r \qquad \text{(Equation G)}$$

where the bivariate estimator, $K_{biv}(r)$, contains two individual bivariate K-functions: $K_{bs}(r)$ calculates the distribution of the big gold particles with respect to each small gold particle whereas $K_{sb}(r)$ computes the distribution of the small gold particles with respect to each big gold particle. A PM sheet area A contains n_b, number of 6-nm gold particles (b = big gold) and n_s, number of 2-nm small gold particles (s = small gold). Other notations are the same as in Equations A and B. $L_{biv}(r)$-r is a linear transformation of $K_{biv}(r)$, and we normalize $L_{biv}(r)$-r against the 95% confidence interval (95% C.I.) estimated from Monte Carlo simulations. Data S1 includes custom algorithms to calculate the bivariate K-function and an estimate of the 95% CI. Under the null hypothesis of no spatial interaction between the two point patterns $L_{biv}(r)$-r has an expected value of 0 for all values of r. Positive deviations of the $L_{biv}(r)$-r function outside of the confidence interval indicate significant co-clustering of the two gold populations. A useful summary statistic to quantify the extent of co-clustering is the area-under-the- $L_{biv}(r)$-r curve over a fixed range $10 < r < 110$ nm which we term the bivariate $L_{biv}(r)$-r integrated, or LBI parameter formally defined as:

$$LBI = \int_{10}^{110} Std\, L_{biv}(r) - r.\, dr. \qquad \text{(Equation H)}$$

For each condition, at least 15 PM sheets were imaged, analyzed and pooled. LBI values < 100 (the 95% C.I.) indicate no significant co-clustering. Although the pooled LBI data are shown as conventional mean ± SEM the LBI parameter is not normally distributed. Therefore the statistical significance of differences between the replicated bivariate point patterns was evaluated in bootstrap tests constructed exactly as described above in Equation C.

Western Blotting to Determine the Activities of the MAPK and PI3K Pathways in Cells

MDCK cells stably expressing K-Ras, K-Ras-K177Q or K-Ras-K178Q were grown to confluence. Cells were serum starved overnight, stimulated with EGF for 5 min, and then harvested. Cells were washed twice with ice cold PBS followed by a 5 min-incubation on ice in 100 μL lysis buffer containing 1% NP40, 50 mM Tris (pH 7.5), 25 mM NaF, 75 mM NaCl, 5 mM $MgCl_2$, 5 mM EGTA, 0.5 μg/ml aproptinin, 0.1 mM Na_3VO_4, 3 μg/ml Leupeptin, 1 mM DTT. Cell lysate was collected into Eppendorf tubes and centrifuged at 1000 RPM at 4°C for 5 min. Supernatant was collected and concentration of total protein was measured. 20 μg of total protein was mixed with sample buffer containing 1 mM Tris (pH6.8), 20 mg/ml SDS, 10% glycerol, 0.5 mg/ml bromophenol blue dye and 15.4 mg/ml DTT. Samples were heated at 95°C for 5 min before being resolved by electrophoresis in a 10% SDS-polyacrylamide gel. Proteins were electro-transferred to polyvinylidene difluoride (PVDF) membrane using pre-chilled transfer buffer containing 3.6 mg/ml glycine, 7.25 mg/ml Tris base, 0.46 mg/ml SDS and 20% methanol. PVDF membranes were rinsed twice with TBST (10 mM Tris (pH 7.5), 150 mM NaCl and 0.1% Tween 20), stained with Coomassie blue (2.4 mg/ml Coomassie BrilliNR Blue, 45% methanol and 10% glacial acetic acid) for 5 min and destained by three washes of 5 min each in 45% methanol and 10% glacial acetic acid. After three washes in TBST (5 min) membranes were blocked for 1 hr in 3% BSA dissolved in TBST for phospho-antibodies or 5% skim milk in TBST for other proteins. Primary antibody labeling was conducted via overnight incubation of the PVDF membrane in blocking solution (TBST with 3% BSA or 5% skim milk) containing primary antibody: α-pERK at 1/3000 dilution, α-pMEK, α-pAkt and α-actin at 1/1000 dilution. The PVDF membrane was then washed three times with TBST (10 min each) before a 1-h incubation with secondary antibody in blocking solution containing 5% skim milk: all anti-rabbit at 1/2,000 dilution. PVDF membranes were washed three times in TBST (10 min each) before a 5 min incubation with enhanced chemiluminescence (ECL) solution: 2 ml SuperSignal West Pico stable peroxide solution and 2 ml SuperSignal West Dura stable peroxide solution. At least 3 independent experiments were conducted. Data are shown as mean ± SEM. Statistical significance was evaluated using one-way ANOVA with * indicating $p < 0.05$.

FLIM-FRET Imaging to Visualize and Quantify the Extent of Aggregation / Co-localization of Proteins and Lipids on the Plasma Membrane

Approximately $2x10^5$ BHK cells were seeded on glass coverslips in 6-well plates on day 1 and transiently transfected with plasmids of GFP-tagged protein alone or co-transfected with combination of plasmids of GFP- and RFP-tagged proteins of interest on day 2. After any treatment, BHK cells were washed twice with PBS at room temperature and then incubated in 4% paraformaldehyde for 30 min in the dark at room temperature. Cells were then washed twice with PBS and quenched in 50 mM NH_4Cl for 10 min, which was followed by 4 times PBS wash and 4 times deionized water wash before being mounted on glass slides using 10.5 μL Mowiol (polyvinyl alcohol 4-88 mounting solution at 10%). Mounted coverslips were then sealed and dried at 37°C for 1 hr before imaging. Fixed and intact BHK cells were imaged using a 60X Plan-Apo/1.40 numerical aperture oil-immersion lens on a Nikon wide-field microscope. Fluorescence lifetime of either GFP or TopFluor-PtdSer was measured using a Lambert Instrument Fluorescence lifetime imaging attachment mounted to the Nikon microscope. FRET efficiency was calculated using Equation I:

$$FRET\ efficiency = \frac{(FL_D - FL_{D/A})}{FL_D} \qquad \text{(Equation I)}$$

where FL_D is fluorescence lifetime of GFP in cells expressing GFP-tagged proteins alone (donor only), $FL_{D/A}$ is fluorescence lifetime of GFP in cells co-expressing GFP-tagged and RFP-tagged proteins (donor-acceptor pair). At least 50 cells were imaged in each condition. Data are shown as mean ± SEM with * indicating statistical significance, $p < 0.05$ evaluated by one-way ANOVA.

Confocal Imaging to Visualize the Intracellular Localization of K-Ras PBD Mutants in Cells

MDCK cells stably expressing indicated mGFP-K-RasG12V PBD mutants were grown to continuous monolayer on glass coverslips, washed twice with PBS at room temperature and fixed with 4% PFA as per the same fixation protocol in the FLIM section above and imaged using a 60X Apo TIRF/1.49 NA oil-immersion lens on a Nikon A1R confocal microscope under a 488 nm diode laser at 20 mW. To quantitate K-Ras mislocalization from the PM the intensity of mGFP pixels in multiple lines scans across the cells were measured using a custom ImageJ algorithm (ver. 2.0). The distribution of mGFP pixel intensities was divided into cytosolic and PM fractions, which were in turn used to calculate the fraction of cytosolic K-RasG12V.

Classical Molecular Dynamics Simulation to Solve the Structures of K-Ras Anchors

We performed atomistic molecular dynamics (MD) simulations on five tK-variants: tK-WT, tK-K177Q, tK-K178Q, phosphorylated tK at S181 (181-Phos) and geranylgeranylated tK (tK-GG). Initial structures for K177Q and K178Q and 181-Phos were derived from the WT tK previously simulated in a POPC/POPG bilayer (Janosi and Gorfe, 2010), where there were four peptides in the simulation box to increase sampling. System construction involved replacing POPG to POPS (Prakash et al., 2016), mutating relevant residues to Q, adding phosphate to Ser181, or replacing farnesyl at position 185 by geranylgeranyl. Parameters of GG were derived from those of farnesyl described in Prakash et al. (2016). The bilayer was symmetric and consisted of 104 POPC/POPS lipids and two peptides per

leaflet in a simulation of box 110x65x95 $Å^3$ containing TIP3P water molecules and neutralizing sodium ions. The total number of atoms in each system was 650,000.

Each peptide-bilayer-water system was energy minimized for 2000 steps with lipid and protein heavy atoms fixed and equilibrated for 200 ps with the lipid phosphate atoms and protein heavy atoms harmonically restrained with a force constant k = 4 kcal/mol/$Å^2$, followed by four 100 ps equilibration steps with a gradually decreasing restraint (k scaled by 0.75, 0.50. 0.25 and 0). The time step used during equilibration was 1 fs. The equilibrated system was simulated with a 2 fs time step using SHAKE to restrain all bonds involving hydrogen atoms and coordinates were saved every 10 ps for analysis. We used particle mesh Ewald (PME) electrostatics and 12 Å and 14 Å cutoffs for non-bonded interactions and pair-list updates, respectively. The NPT ensemble was used, with constant pressure of 1 bar maintained by the Nose-Hoover Langevin piston method and temperature of 310 K controlled by the Langevin thermostat method. The force field was CHARMM27 (MacKerell et al., 1998) for proteins and CHARMM36 for lipids (Klauda et al., 2010). Simulations were conducted with the NAMD2.9 program (Phillips et al., 2005) for 1 μs.

The trajectories were used to examine equilibrium and time-dependent properties of the peptides and the bilayer after excluding the initial 100 ns that was considered an equilibration phase. Our analysis involved standard measures such as root mean square deviation (RMSD), radius of gyration and number of hydrogen bonds as well as less common ones such as relative free energy profile. For analysis of peptide structure and energetics in a statistically significant manner a single large trajectory was derived by concatenating the trajectory of each peptide within a simulation box, which yielded an aggregate simulation time of 4 μs per sequence. For tK-WT, we also analyzed trajectories (aggregate length 4 μs) extracted from previous simulations of full-length K-Ras in the same bilayer system (Prakash et al., 2016). Classification of the structure into ordered (O), disordered (D) and intermediate (I) groupings was achieved by analyzing the probability distribution of the RMSD of residues 177-182. Where applicable, the probability was converted to a free energy profile through $\Delta G = -RT\ln(p)$, where p is the population density, R is the gas constant, T = 310K is temperature. 2D radial pair distribution function ($g_{2d}(r)$) was used to evaluate the distribution of lipid head group oxygen atoms around nitrogen of Lys and oxygen of Ser/Thr side chains. To avoid effects from membrane undulation, the $g_{2d}(r)$ was computed using a relatively short segment of the simulations (the last 500 ns). All of the analyses and visualization were conducted with the program VMD (Humphrey et al., 1996) and VMD-compatible in-house tcl scripts.

Metadynamics Simulations to Calculate the Conformational Transitions of K-Ras Anchors

The enhanced sampling method metadynamics (metaMD) was used to sample conformational transitions of tK and its variants bound to model membrane. MetaMD applies a time-dependent biasing potential along a set of collective variables (CVs) by adding Gaussians to the total potential in order to overcome barriers larger than kT (Barducci et al., 2011; Laio and Parrinello, 2002). The bias potential $V_{meta}(\xi(t))$ is given by:

$$V_{meta}(\xi(t)) = \sum_{t_0=0,\delta t,2\delta t}^{(t-\delta t)} w \prod_{k=1}^{N_{cv}} \exp\left(-\frac{(\xi_k(t)-\xi_k(t_0))^2}{2\delta\xi_k^2}\right), \qquad \text{(Equation J)}$$

where w is a constant with the dimension of energy, $\xi_k(t)$ is the value of the k^{th} CV at time t, and $\xi_k(t_0)$ is its value at the previous time t_0. $\delta\xi$ is a user-defined half-width of the Gaussian along the direction of the CV, and N_{CV} is the number of CVs used.

The choice of CV is extremely important. A good CV must be able to distinguish between the initial and final states while describing all relevant intermediate states. In the current work, we used a detailed analysis of a combined 8 μs unbiased cMD data (Figures 4A and S4) and a series of trial and error experimentations to arrive at two CVs: the Cα-atom RMSD of residues 177-182 from a helical reference structure (CV1) and the end-to-end distance involving the Cα atom of residues 176 and 184 (CV2). Before settling on these CVs, we conducted both regular and well-tempered metaMD with RMSD as a reaction coordinate, applied to the wild-type tK bound to membrane. We found that even after a microsecond or longer run the free energy surface (FES) did not become flat and the dynamics did not become diffusive. One reason could be the fact that conformers with different global shape can have the same RMSD. Another potential reason is that the coupled dynamics of the bilayer and peptide may not be effectively captured by the peptide's RMSD alone. The challenge of convergence of metaMD is well known, especially when applied to systems such as the adsorption of peptides on organic or bilayer surfaces (Deighan and Pfaendtner, 2013) and sampling of conformational dynamics of a peptide bound to membrane bilayer (Cui et al., 2011). The use of more than one CV often helps to cross barriers and achieve convergence. In our search for a second CV, we tested a number of parameters including the radius of gyration, number of peptide-lipid hydrogen bonds, and helicity. Some of these, particularly radius of gyration, appeared to be working. However, we noticed that the curled or ordered form of our peptide differs in its capacity to form hydrogen bonds with bilayer lipids when compared with the extended conformation (Figure 4C). We therefore reasoned that an end-to-end distance might be able to effectively capture both the dynamics of the peptide and its interaction with lipids.

All metaMD simulations were performed using the COLVARS module in NAMD (Fiorin et al., 2013). The lower and upper bounds of CV1 were set to 0 and 4.2 Å, and those of CV2 were set to 7 and 23 Å; these ranges were based on analysis of our unbiased cMD data (Figures 4 and S4). A repulsive wall with a force constant of 1000 kcal/mol was applied at the upper boundaries. For each system, a single peptide (tK or its variants) was embedded in a relatively small symmetric bilayer of 104 lipids (80 POPC and 24 POPS), solvated in a box of ~60 × 60 × 90 $Å^3$ containing charge-neutralizing Na^+ and Cl^- ions. The total system size ranged from 31,000 to 33,000

atoms. The system was equilibrated for 0.5–1 ns under NPT ensemble using the protocol used in our cMD runs (i.e., PME electrostatics, and 12 Å and 14 Å cutoffs for non-bonded interactions and pair-list updates). After this equilibration phase, we switched to NVT and ran metaMD using a hill height of 0.5 kcal/mol and a 0.02 Gaussian width for both CV1 and CV2, with the frequency of deposition of Gaussians being every 1 ps. The total metaMD lengths ranged from 1.2 μs to 1.6 μs, with the actual duration being determined by the extent of convergence monitored as described below. The PMF was written out every 10 ns.

Convergence of metaMD depends on the number of transition events between states and sampling of all physically interesting regions of the CV. Convergence can be evaluated in different ways including by monitoring the stability of free-energy differences between different states (Deighan and Pfaendtner, 2013; Limongelli et al., 2013). Following these previous reports, we checked convergence by (1) calculating the free-energy difference, $\Delta G_{D\text{-}O}$, between the two lowest free-energy basins representing the disordered (D) and ordered (O) states and (2) comparison with our unbiased cMD for WT tK. The latter indicated that the 2D PMFs of tK derived from metaMD and cMD share remarkable similarity (Figure S4C). The cMD FES reveals three minima at RMSD values of about 0.5 Å, between 1 and 1.5 Å and > 2.0 Å, each of which are also found in the FES obtained from metaMD. The former entailed deriving a 1D PMF along the CV1 or CV2 from the 2D FES using the relation:

$$P(s) = \frac{\exp(-F(s)/k_B T)}{\sum_s \exp(-F(s)/k_B T)}; \quad \text{(Equation K)}$$

$$F(s) = -1/\beta \log P(s) \quad \text{(Equation L)}$$

where F(s) is the value of the free energy (PMF) at s, T is temperature in Kelvin and β is the Boltzmann's constant. Figure S4B plots $\Delta G_{D\text{-}O}$ along RMSD for the five metaMD simulations. In each case, the $\Delta G_{D\text{-}O}$ changed little over at least a 300 ns time period at the end of the simulations. Taken together, we believe our metaMD runs are sufficiently converged to yield reliable conformational energy landscapes.

Comparison of the final free energy surfaces shown in Figure S4C indicate that, relative to the wild-type peptide, 181-Phos and tK-GG strongly favor the D state whereas the Q mutations at positions 177 and 178 shift the equilibrium toward the ordered or semi-ordered states, consistent with the cMD results. Note that the simulations discussed above were all started from a D conformation. Test simulations on Phos-181 and tK-GG started from an O conformation led to a very fast transition to the D state (within 100 ns). This provides additional support to our conclusion that these two peptides favor the disordered conformation.

Reverse Phase Protein Array (RPPA) to Quantify Effects of Polybasic Domain Mutations on Signal Output

BHK cells were transiently transfected with GFP-tagged K-RasG12V or K-RasG12V PBD single point mutants (K175Q, K176Q, K177Q, K178Q, K179Q or K180Q). Whole cell lysates containing 40 μg of total proteins were collected after over-night serum-starvation. The Reverse Phase Protein Array (RPPA) was conducted by the RPPA Core Facility at the M. D. Anderson Cancer Center (Houston, Texas, USA) according to their published protocols using 297 validated antibodies to quantify protein levels. Relative protein levels for each sample were determined by interpolation from the standard curve of each antibody and normalized for protein loading. Raw values were then converted to Log2 values and shown as a heatmap, which is centered at 50 percentile (white) and with a range of −0.3 (blue) and 0.3 (red). We show data for 60 phospho-proteins in the heat-maps in main Figure 6 and 274 proteins in Figure S6. Hierarchal clustering of the larger dataset in Figure S6 was using Pearson Correlation and a center metric, which is visualized in TreeView.

Lipidomics to Monitor the Extent of Acyl Chain Modification of Exogenous PtdSer Species after Uptake by BHK Cells

Synthesized or extracted PtdSer species were purchased from Avanti Polar Lipids as solution dissolved in chloroform at 5 mg/ml and stored at −20°C under N_2. On the day before experiment, appropriate amount of lipid/chloroform solution was transferred to a 20 ml glass vial using a glass Hamilton syringe. Cholorform was evaporated via purging of N_2. The glass vial containing a PtdSer lipid film then placed in a vacuum desiccator overnight to eliminate the residue chloroform. On the day of supplementation experiment, appropriate amount of medium containing full serum was added to the dried lipid film in the glass vial, which was then sonicated for 20 min using a bath sonicator before supplementation.

BHK cells were treated with 10 μM fendiline for 24 hr before 1 hr incubation with various 10 μM exogenous PtdSer species. Cells were then trypsinized using 1X trypsin-EDTA and washed twice with ice-cold PBS. Cells were resuspended in PBS and cell number was counted using a Countess automated cell counter (Invitrogen). Final concentration was 450,000 cells / 300 μL PBS for all samples, which were frozen at −80°C and shipped to Lipotype GmbH, Germany, for detailed lipidomics analysis. Three independent experiments were performed and analyzed. Data are shown as mean ± SEM in Figure S2G. Statistical significance between different lipid supplementation was evaluated using one-way ANOVA, with * indicating $p < 0.05$.

QUANTIFICATION AND STATISTICAL ANALYSIS

Two main statistical analyses were used. Bootstrap tests as described above were used to examine for statistical differences between replicated point patterns in the EM univariate and bivariate K-function analyses. One-way ANOVA was used for other datasets. The analysis used and the p values are indicated in the figure legends.

DATA AND SOFTWARE AVAILABILITY

Algorithms to calculate univariate and bivariate K-functions, and an ImageJ algorithm to estimate mislocalization of K-Ras from the plasma membrane are supplied in Data S1.

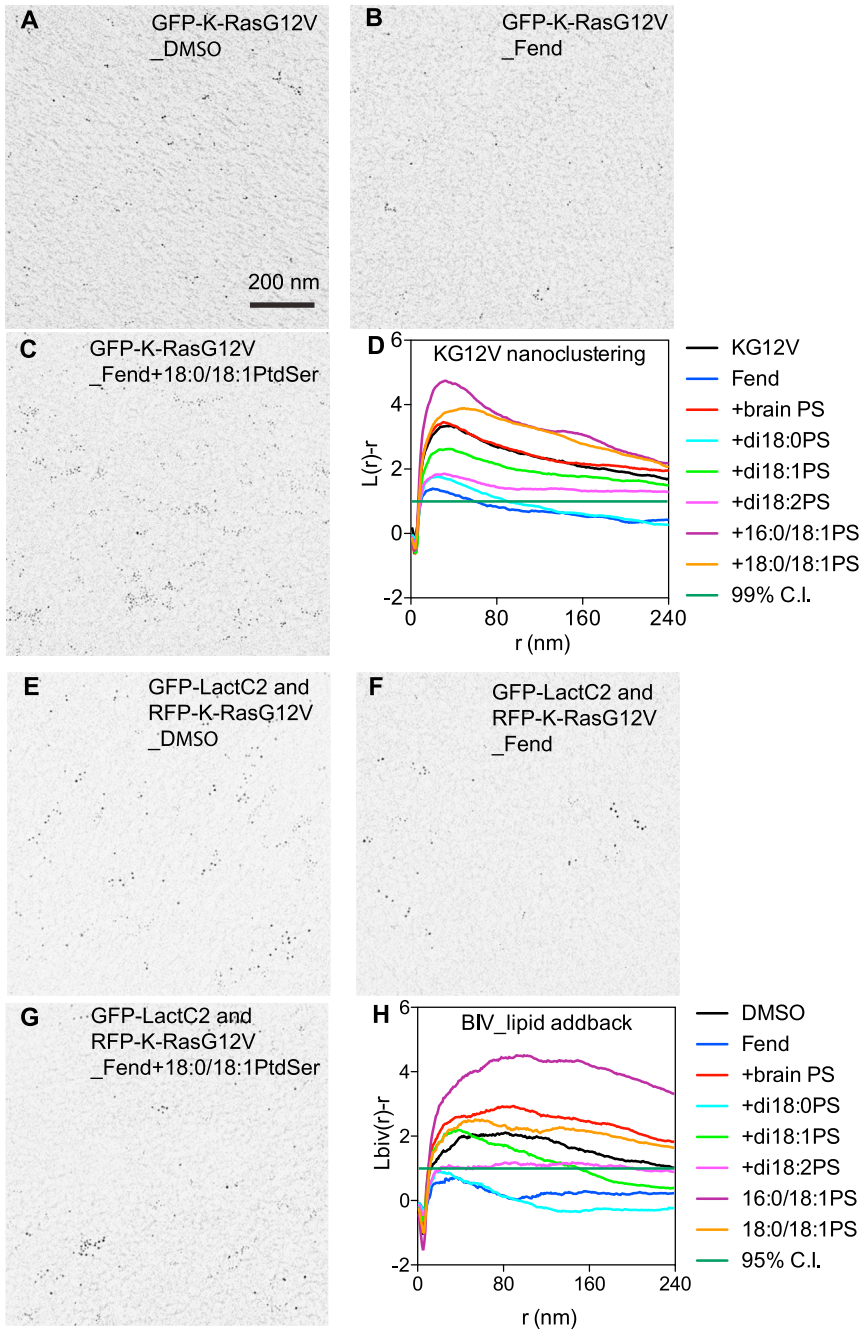

Figure S1. EM Univariate and Bivariate Spatial Analysis, Related to Figure 1

Sample EM images of 1 μm^2 area of the inner PM leaflet of BHK cells expressing GFP-K-RasG12V and treated (A) with vehicle DMSO, (B) with 10 μM fendiline or, (C) with fendiline followed by 1 hr supplementation with exogenous 18:0/18:1 PtdSer. In each case GFP-K-RasG12V was labeled with 4.5 nm gold coupled to anti-GFP antibody. (D) Weighted mean univariate K-function curves ($n \geq 15$) of immunogold labeled GFP-K-RasG12V under control, fendiline treatment (Fend) and fendiline treatment followed by supplementation with different PtdSer species. Sample EM images of 1 μm^2 area of the inner PM leaflet of BHK cells co-expressing GFP-LactC2 and RFP-K-RasG12V treated with (E) vehicle DMSO, (F) 10 μM fendiline or (G) fendiline followed by 1 hr supplementation with exogenous 18:0/18:1 PtdSer. GFP-LactC2 was labeled with 6 nm gold coupled to anti-GFP antibody and RFP-K-RasG12V was labeled with 2 nm gold linked to anti-RFP antibody. (H) Weighted mean bivariate K-function curves ($n \geq 15$) showing the extent of co-localization between 2 nm and 6 nm gold particles under fendiline treatment (Fend) and fendiline treatment followed by supplementation with different PtdSer species.

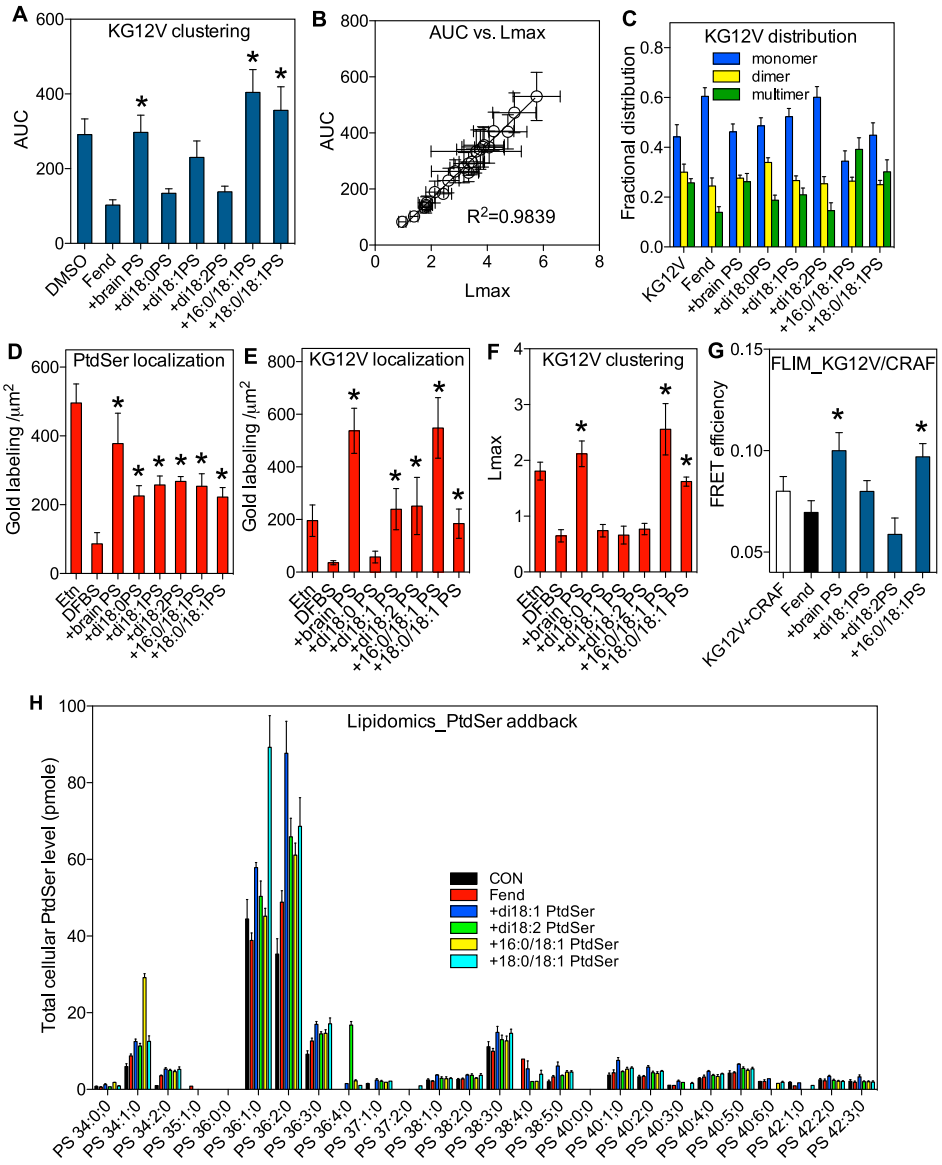

Figure S2. Response of GFP-K-RasG12V to Exogenous PtdSer, Related to Figures 1 and 2

(A) Area-under-the-curve values (AUC) for GFP-K-RasG12V were derived from the univariate K-function curves shown in Figure S1D. The responses quantified by the AUC parameter exactly mirror the changes in L_{max} values shown in main Figure 1. (B) AUC values calculated from univariate K-function curves shown in Figure 1 and Figure 2 were correlated with the corresponding L_{max} values. (C) Fractional distribution analysis of GFP-K-RasG12V on the PM using data shown in main Figures 1C and 1E. (D) PSA3 cells expressing GFP-LactC2 were grown in dialyzed FBS with or without 10 μM ethanolamine (Etn) for 72 hr before incubation with various PtdSer species for 1 hr. GFP-LactC2 PM localization was evaluated as gold particle labeling density after anti-GFP immuno-gold labeling conducted as in Figure 1. Identical PtdSer add-back experiments were conducted in Etn-starved PSA3 cells expressing GFP-K-RasG12V. GFP-K-RasG12V PM localization (E) and nanoclustering (F) were analyzed using univariate K-function ($n \geq 15$ for each condition) after anti-GFP immunogold labeling of PM sheets, again as in Figure 1. Results are shown as means ± SEM. Statistical significance of differences was evaluated using one-way ANOVA for PM localization and in bootstrap tests for nanoclustering (*$p < 0.05$). (G) BHK cells co-expressing GFP-K-RasG12V and RFP-CRAF were treated with vehicle (DMSO) or 10 μM fendiline for 24 hr before 1 hr incubation with exogenous PtdSer. Cells were imaged in a wide-field FLIM microscope to measure GFP fluorescence lifetime. FRET efficiencies between GFP-K-RasG12V and RFP-CRAF were calculated. Approximately 60 cells were imaged for each condition. Statistical significance was evaluated by one-way ANOVA (*$p < 0.05$). (***H***) Potential lipid acyl chain remodeling of exogenous PtdSer lipids was evaluated using lipidomics. BHK cells were treated with 10 μM fendiline for 48 hr, which compromises endolysomal function to extensively redistribute PtdSer away from the PM and modestly reduce total PtdSer levels (Cho et al., 2015; Zhou et al., 2014) and then incubated for 1 hr with various exogenous PtdSer species before harvesting and freezing at −80°C. Whole cell extracts were comprehensively analyzed for each PtdSer species by quantitative mass spectrometry. Three independent experiments were performed and results are mean ± SEM. PtdSer was abbreviated as PS in plots.

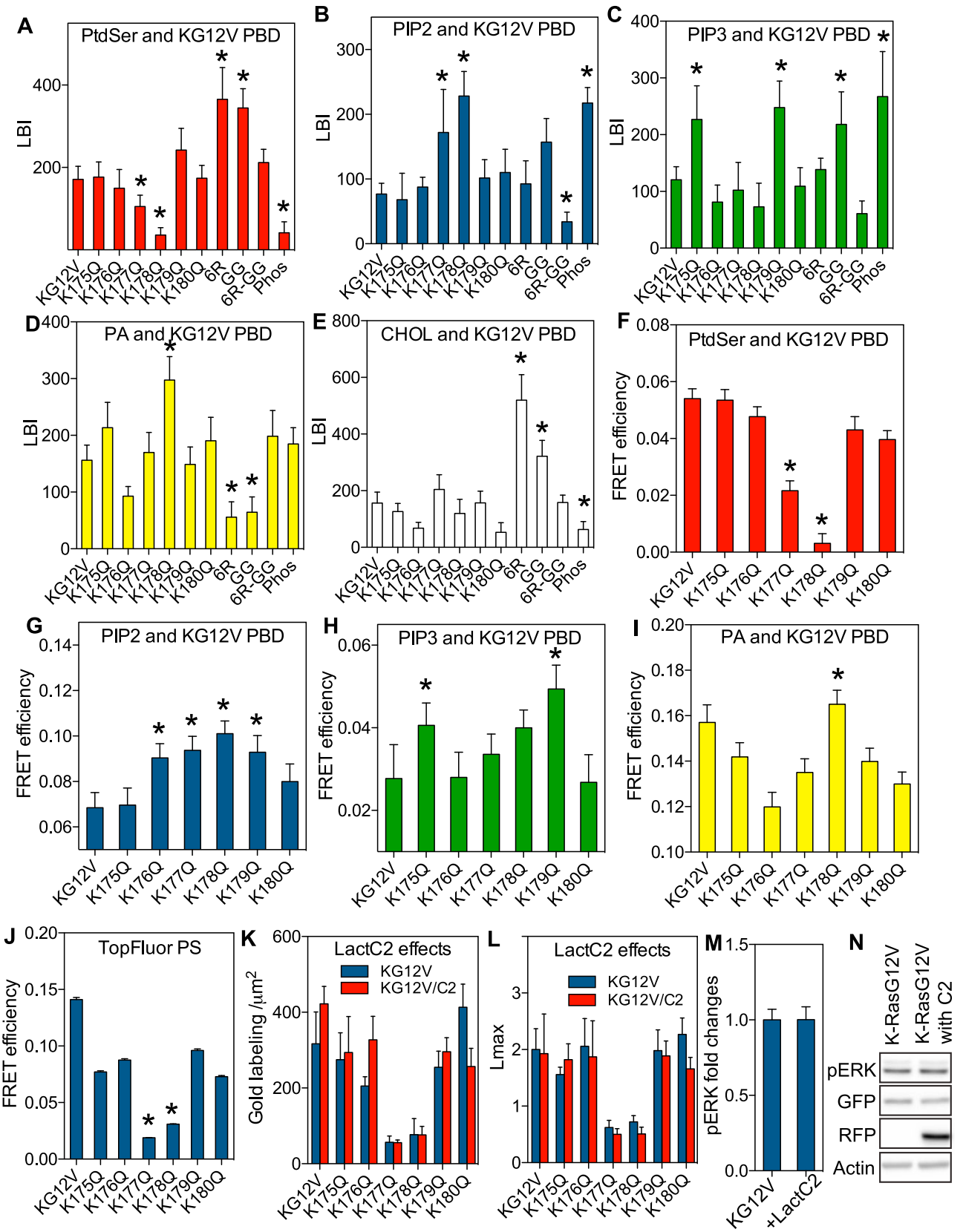

(legend on next page)

Figure S3. Spatial Analysis of K-RasG12V PBD Mutants, Related to Figures 1 and 2

(A–E) LBI values used to construct the heatmap summary in main Figure 2. Data are shown as mean ± SEM ($n \geq 15$ images for each condition), with statistical significance of differences evaluated using bootstrap tests. (F–I) Extent of lipid / K-RasG12V co-localization was validated using FLIM-FRET in intact BHK cells co-expressing each GFP-lipid binding domain and each RFP-K-RasG12V PBD mutant. FRET efficiency was calculated from GFP fluorescence lifetime. Data are shown as mean ± SEM ($n \geq 50$ cells for each condition), with statistical significance of differences evaluated using one-way ANOVA (*$p < 0.05$). The EM and FLIM data are generally closely concordant. The small discrepancies between the datasets likely originate from the different length scales evaluated by the two techniques. EM-bivariate analysis measures the extent of co-clustering over a more extensive range of length scales than does FRET, which is restricted to when the donor and acceptor molecules are within 10 nm of each other. (J) FRET efficiency between TopFluor PtdSer, an acyl chain-modified fluorescence PtdSer, and RFP-K-RasG12V PBD mutants was calculated from measurements of the fluorescence lifetime of TopFluor made by FLIM. At least 50 cells were imaged for each condition and results show mean ± SEM. The potential effects of expressing the PtdSer-binding domain GFP-LactC2 on K-RasG12V PBD PM interactions were systematically examined in EM experiments. (K) GFP-K-RasG12V localization to the PM without/with RFP-LactC2 was counted within a 1 μm^2 area of the inner PM leaflet of BHK cells. (L) Extent of univariate nanoclustering of GFP-K-RasG12V was analyzed in BHK cells expressing GFP-K-RasG12V polybasic domain mutants without / with RFP-LactC2 ($n \geq 15$ for each condition). Statistical significance was evaluated using bootstrap tests. (M and N) K-RasG12V signal transduction was measured in BHK cells expressing GFP-K-RasG12V without / with RFP-LactC2. Quantitative western blotting was conducted using antibodies against phosphorylated ERK, GFP, RFP and actin as loading control.

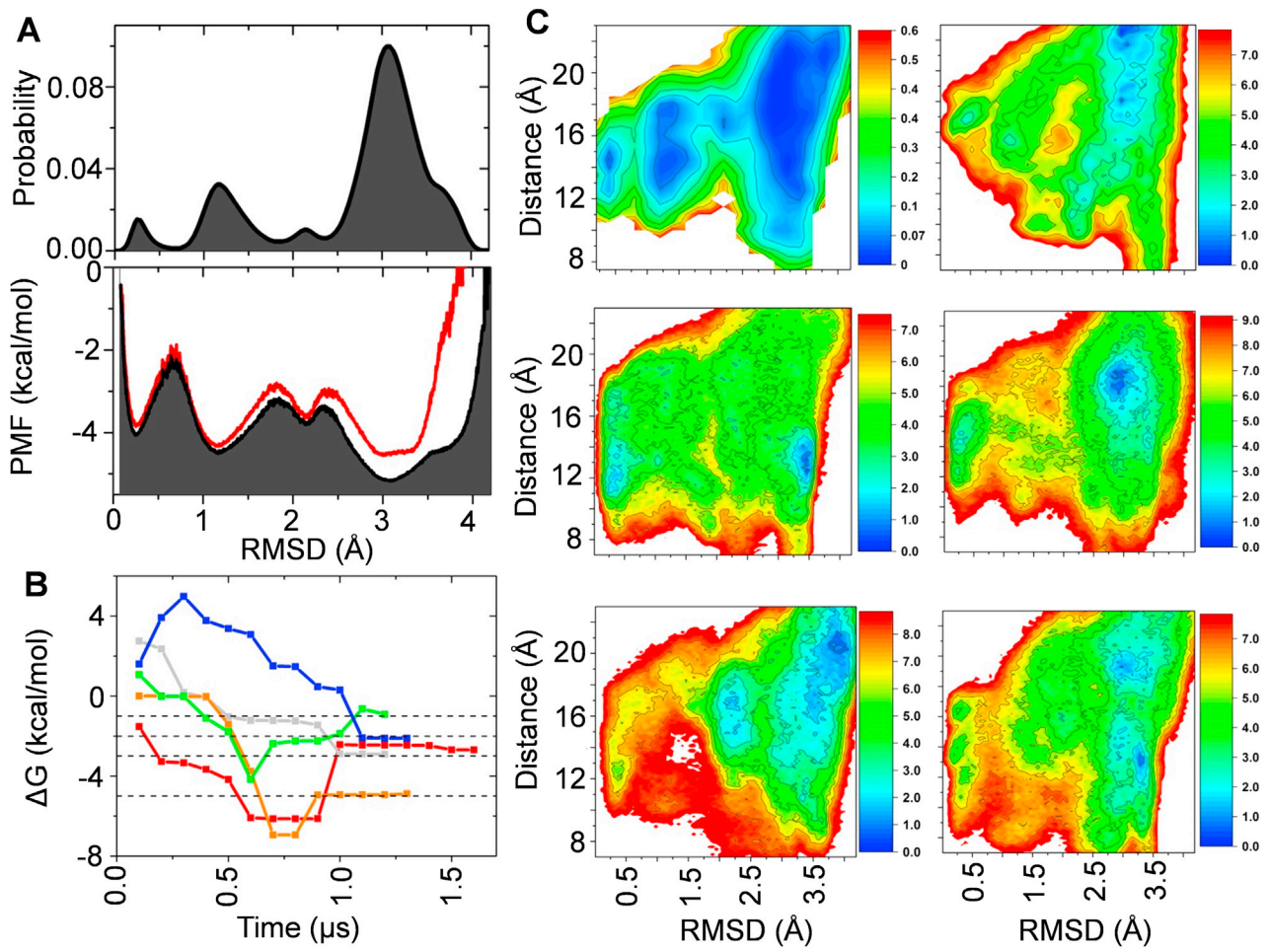

Figure S4. Energy Landscapes, Related to Figure 4

(A) Top: the probability distribution of C_α atom RMSD (residues 177-182) from cMD of the isolated WT tK plus data extracted from cMD of full-length K-Ras from (Prakash et al., 2016) (8 μs total simulation time); Bottom: PMF along RMSD obtained by Boltzmann inversion of the probability distribution. For reference, the PMF from only the 4 μs cMD data of the isolated WT tK is shown in red. (B) Convergence of metaMD based on the free energy difference between the two lowest energy basins: the disordered state D and ordered state O ($\Delta G_{O\text{-}D}$). The 1D PMF as a function of RMSD used for these calculations was obtained from reweighting the 2D metaMD PMF profiles shown in (C, last five panels). Shown in the first panel of (C) is a 2D PMF from the histogram of RMSD versus distance between C_α atoms of residues 176 and 184 derived from the cMD data described in (A). Color code in (B): WT tK (red), tK-K177Q (green), tK-K178Q (blue), 181-Phos (orange) and tK-GG (gray).

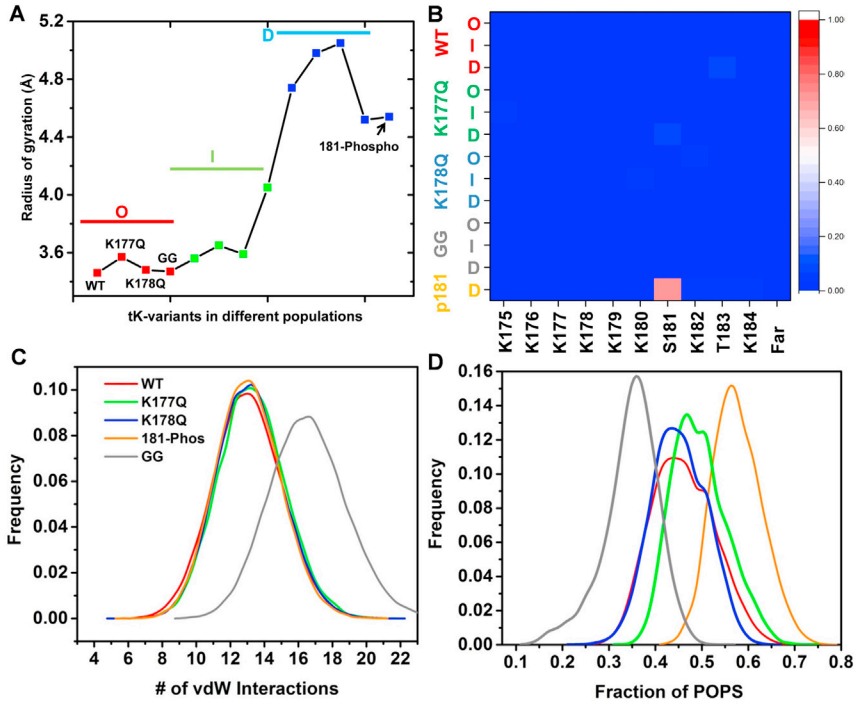

Figure S5. Radius of Gyration of the Different Structural Classes of tK-WT, tK-K177Q, tK-K178Q, and tK-GG, and Probability Distribution of PBD-Lipid Interactions, Related to Figure 5

(A) In each case, the ordered O structures are compact, the intermediate I structures are slightly less compact while the disordered D structure are extended. (B) The probability of peptide-PtdSer hydrogen bonding interactions with the peptide as acceptor, showing that PtdSer donates hydrogen only to the phosphate oxygen atoms of 181-Phos. (C) The number of peptide-lipid carbon-carbon contacts (vdW interactions) calculated as the number of lipid tail carbon atoms within 4 Å of any peptide carbon atom. (D) The fraction of PtdSer around the PBDs, calculated as the ratio of the number of interactions of the peptide with PtdSer over its interactions with any lipid. Interaction was defined to exist if any heavy atom of a lipid is within 4 Å of any heavy atom of peptide.

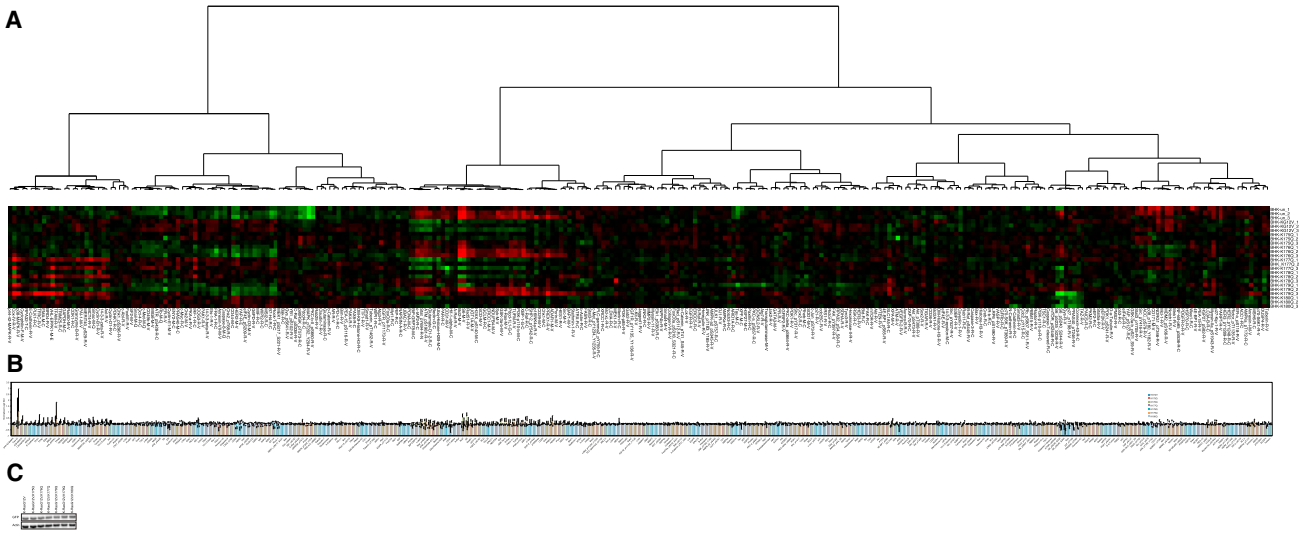

Figure S6. Functional Consequences of K-Ras PBD Mutations, Related to Figure 6

(A) BHK cells transiently transfected with different GFP-K-RasG12V PBD mutants were serum-starved overnight before harvesting. Whole-cell lysates were analyzed using reversed phase protein arrays. Protein levels were calculated using internal standard curves and normalized linear values were transformed into Log2-based values shown. Three independent experiments were conducted. The heatmap shows data from individual experiments (A) and a bar chart showing mean log2 fold changes ± SEM is shown in (B). The data in main Figure 6 show changes in phosphorylated-proteins only, this figure shows all protein levels assayed. Hierarchal clustering of changes in protein levels was carried out using Pearson Correlation and a center metric, which is visualized in TreeView. (C) Expression levels of GFP-K-RasG12V PBD mutants in BHK cells used for RPPA assays were quantified using western blotting.